Electron paramagnetic resonance study of gadolinium in Czochralski-grown yttrium fluoride single crystals

1999 J. Phys.: Condens. Matter 11 7211

(http://iopscience.iop.org/0953-8984/11/38/302)

J. Phys.: Condens. Matter **11** (1999) 7211–7217. Printed in the UK PII: S0953-8984(99)04331-3

Electron paramagnetic resonance study of gadolinium in Czochralski-grown yttrium fluoride single crystals

K J Guedes†, K Krambrock† and J Y Gesland†‡

† UFMG, Departamento de Física, ICEx, CP 702, 30.123-970 Belo Horizonte, Brazil
‡ Equipe de Physique de l'Etat Condensé, CNRS URA No 807 Avenue Messiaen, BP 535, 72017 Le Mans Cédex, France

Received 14 May 1999, in final form 12 July 1999

Abstract. Single crystals of YF_3 grown by the Czochralski method have been investigated by electron paramagnetic resonance (EPR). In this paper we present an EPR analysis of residual Gd^{3+} impurities. We found that the Gd^{3+} rare-earth ion substitutes for Y^{3+} in YF_3. Detailed analysis of the EPR spectra allowed us to determine the fine structure parameters of Gd^{3+} in monoclinic C_s site symmetry. The EPR angular dependence is dominated by the electronic quadrupole tensor; the g-factor is slightly axial. The b_2^0 parameter found for Gd^{3+} in YF_3 is unexpectedly high when compared to Gd^{3+} in the hosts of LaF_3 structure where the coordination number is the same. The results let us conclude that YF_3 is a promising laser host crystal.

1. Introduction

It is well known that fluoride materials can be used as active media for tunable solid state lasers. In particular lithium yttrium fluoride $LiYF_4$ and potassium yttrium fluoride KY_3F_{10} doped with rare-earth ions or transition metals are used for applications in this field. It seems that yttrium fluoride YF_3 could be also a laser material [1]. In this work we report on the growth and the characterization of Czochralski-grown YF_3 single crystals by electron paramagnetic resonance (EPR). In the EPR spectra at room temperature residual Gd^{3+} impurities have been observed. To our knowledge, no EPR experiment has been reported on Gd^{3+} in YF_3 previously. From the technological point of view the EPR experiments are interesting, since a large value of the b_2^0 fine structure parameter indicates that the material in investigation is a promising laser host crystal [2–4]. Recently, it has been shown that Nd in YF_3 has an interesting vacuum ultraviolet fluorescence spectrum [5].

2. Experiment

The growth of single crystals of YF_3 by the Czochralski method is impossible directly from the melt at 1435 K. The reason is a drastic high temperature phase transition at about 1350 K known as the α–β transition from rhombohedral to orthorhombic symmetry. However, by a special process using a mixture of 0.8 YF_3 and 0.2 LiF large single crystals of YF_3 were grown directly in the β-phase, at 1060 °C [6]. The orthorhombic YF_3 crystals are non-hygroscopic and colourless under normal conditions essential for use as active laser materials. More details of the growing procedure can be found elsewhere [6].

0953-8984/99/387211+07$30.00

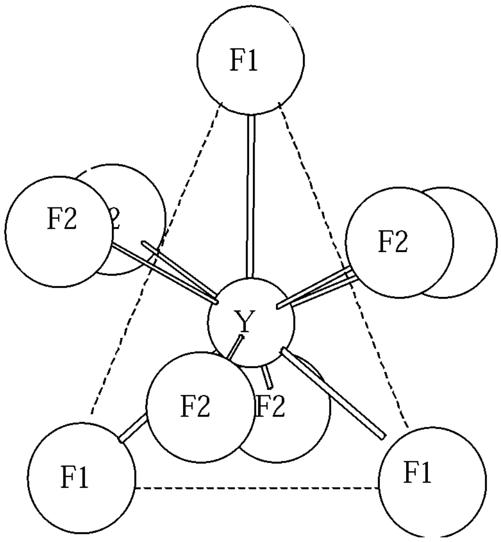

Figure 1. The coordination of Y in YF_3. The plane defined by the three F1 is the mirror plane *ac*.

YF_3 at room temperature exhibits an orthorhombic structure with space group P_{nma} (D_{2h}^{16}) with four molecules per unit cell [6, 7]. It is known as the β-YF_3 type with lattice parameters [7]: $a_0 = 6.3537$ Å, $b_0 = 6.8545$ Å, $c_0 = 4.3953$ Å, a slightly distorted LaF_3 hexagonal lattice. In this structure, each Y^{3+} ion is surrounded by eight fluorine ions at similar distances and with a ninth fluorine at a greater distance as shown in figure 1. The plane defined by the three fluorine F1 corresponds to the mirror plane *ac*. Six of the nine fluorine ions (F2 type) are at the corners of an irregular trigonal prism with a yttrium in the centre. The three fluorine F1 are in front of the three lateral faces of this trigonal prism, so that the coordination polyhedron has the shape of a tricapped prism. These polyhedra form cycles of six prisms; four of them share faces while the others are linked by edges.

For the EPR experiments samples of dimensions of $3 \times 2 \times 5$ mm^3 have been cut with the faces normal to the crystallographic axes using the cleavage plane (100). The orientations of the crystals have been confirmed by the Laue x-ray analysis. EPR spectra were recorded at room temperature using a spectrometer equipped with a cylindrical cavity (Bruker) operating at a microwave frequency of approximately 9.38 GHz with the common 100 kHz field modulation and lock-in detection. A Varian magnet with nine inch pole pieces was used to provide magnetic fields up to 8.5 kG. The field strength was controlled by a proton nuclear magnetic resonance probe. The low temperature experiments have been done with a liquid helium flux cryosystem (Oxford). The EPR spectra were measured for rotations of the crystal in all three orthorhombic planes (*ab*, *ac*, *bc*).

3. Experimental results

Figure 2 shows the X-band EPR spectrum of a YF_3 single crystal for $\boldsymbol{B} \| \boldsymbol{b}$ measured at room temperature with a microwave frequency of 9.38 GHz. The spectrum consists of seven EPR lines with unequal intensities consistent with the spectrum expected for an impurity with $S = 7/2$ split by the fine structure. The EPR lines correspond to $\Delta M_S = \pm 1$ transitions. The spectra were recorded even at room temperature indicating a fairly large spin–lattice relaxation

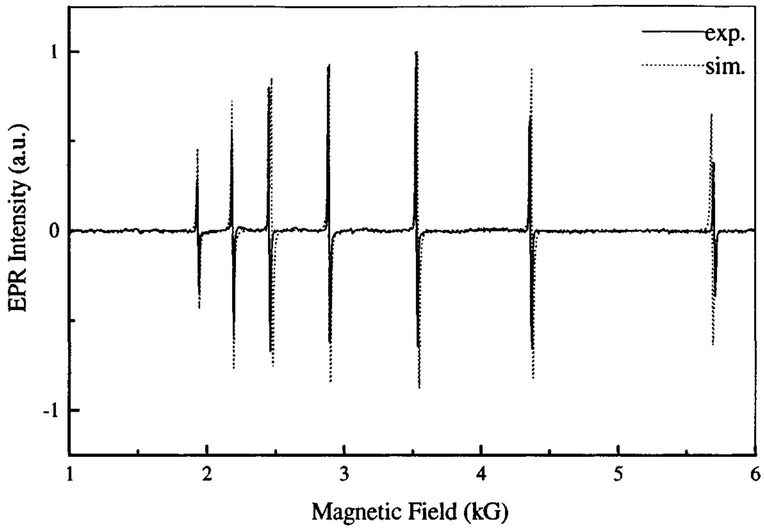

Figure 2. EPR spectrum of Gd^{3+} in a single crystal YF_3 (solid line) obtained for $\boldsymbol{B}\|\boldsymbol{b}$ measured at room temperature and 9.38 GHz together with a computer simulation (dotted line).

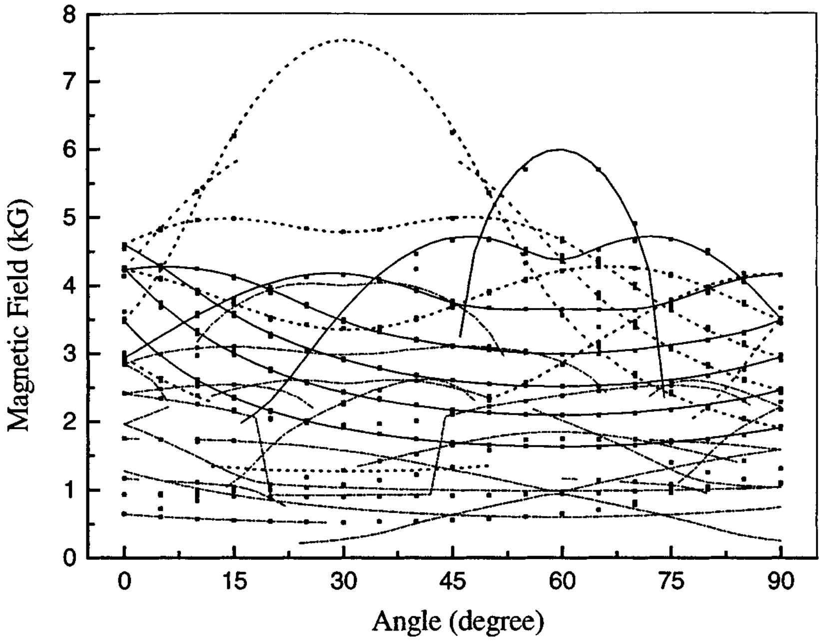

Figure 3. Angular variation of the X-band EPR spectra in the *ac* plane for Gd^{3+} in a YF_3 single crystal at room temperature: $\theta = 0^\circ$ corresponds to c and $\theta = 90^\circ$ to a. The solid and dotted lines are fitted curves that connect data points from the same transition $\Delta M_S = \pm 1$ for two set of magnetically inequivalent ions. They are related by a rotation of 120° in this plane. The chain lines belong to non-allowed transitions of type $|\Delta M_S| \geqslant 2$.

time. The EPR line widths at room temperature are about 10 G. All these observations are consistent with the rare-earth ion Gd^{3+}. The ground state of Gd^{3+} is $(4f^7)$ $^8S_{7/2}$. In a

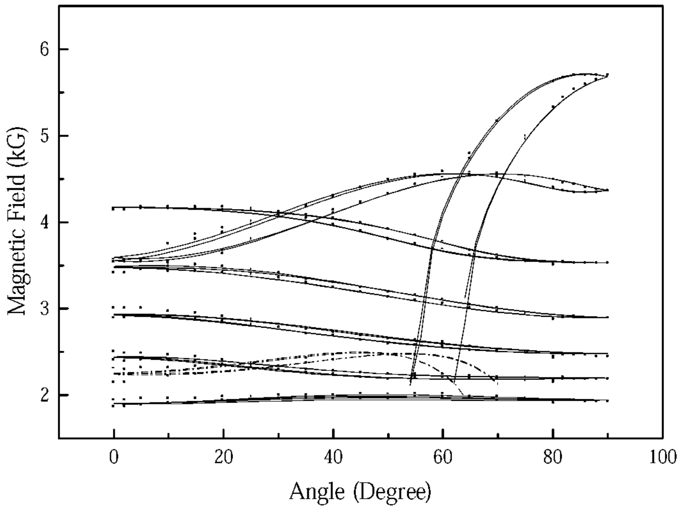

Figure 4. Angular variation of the X-band EPR spectra in the ab plane for Gd^{3+} in a YF_3 single crystal at room temperature. The solid lines are fitted curves that connect data points from the same transition $\Delta M_S = \pm 1$ for two set of equivalent ions. $\theta = 0^\circ$ and $\theta = 90^\circ$ correspond to a and b axes, respectively. The chain lines belong to non-allowed transitions of type $|\Delta M_S| \geqslant 2$.

crystalline field, the eightfold degeneracy is partly removed owing to the admixture with higher states resulting in a set of four twofold levels [8, 9]. For a low symmetry case like YF_3 the degeneracy is totally removed, leading to seven fine structure EPR lines. The gadolinium may come from traces in the raw material Y_2O_3, which had a purity of 99.999% [6]. From our EPR measurements in comparison with a standard sample we estimate the Gd concentration, however, to be two orders of magnitude less (about 10^{15} cm^{-3}).

The angular variation of the EPR spectra in the ac plane from $\theta = 0^\circ$ to $\theta = 90^\circ$ is shown in figure 3. In the figure the dots correspond to EPR line positions and the solid and dotted lines to a computer analysis using an appropriate spin Hamiltonian for the symmetry of the yttrium site in the YF_3 crystal structure, which is described below. The two spectra (dotted lines and solid lines) correspond to two magnetically inequivalent Gd sites and belong to transitions of type $\Delta M_S = \pm 1$. The chain lines are related to non-allowed transitions of type $|\Delta M_S| \geqslant 2$. The high field EPR lines were difficult to analyse because their intensities diminish rapidly with the angular variation. Figure 4 shows the angular variation of the EPR spectra in the ab plane from $\theta = 0^\circ$ to $\theta = 90^\circ$. For $\boldsymbol{B}$ along the crystallographic axis $\boldsymbol{b}$ ($\theta = 90^\circ$) seven fine structure lines are observed (see also figure 2). When rotating the crystal in the ab plane, the seven fine structure lines split into doublets. The splitting of the EPR lines into doublets is discussed below.

4. Discussion

The spin Hamiltonian consistent with Gd^{3+} in the crystal structure of YF_3 in the notation of Abragam and Bleaney [10] is as follows:

$$H = \beta \vec{H} \overleftrightarrow{g} \vec{S} + \sum_{m=0,\pm1,\pm2} \frac{1}{3} b_2^m O_2^m + \sum_{m=0,\pm2,\pm4} \frac{1}{60} b_4^m O_4^m + \sum_{m=0,\pm2,\pm4,\pm6} \frac{1}{1260} b_6^m O_6^m \qquad (1)$$

Table 1. Values of the spin Hamiltonian parameters with g-factor and fine structure parameters b_l^m, ($l = 2$ and 4, $|m| \leqslant l$) expressed in GHz.

$g_{xx} = 1.984 \pm 0.001$	$g_{yy} = 1.983 \pm 0.001$	$g_{zz} = 1.999 \pm 0.001$
$b_2^0 = -1.992 \pm 0.003$	$b_2^1 = -0.036 \pm 0.006$	$b_2^2 = 0.108 \pm 0.003$
$b_2^{-1} = -0.43 \pm 0.02$	$b_2^{-2} = 0.003 \pm 0.003$	
$b_4^0 = 0.0019 \pm 0.0009$	$b_4^2 = -0.059 \pm 0.003$	$b_4^4 = 0.053 \pm 0.003$
$b_4^{-2} = -0.008 \pm 0.006$	$b_4^{-4} = -0.005 \pm 0.005$	

with $S = 7/2$. The first then is the Zeeman term which describes the interaction between the electron spin S and the applied external magnetic field $\boldsymbol{B}$; the remaining terms relate to the splitting of the electronic levels in zero magnetic field. The spin operators O_l^m are functions of degree l of the angular momentum operator S_Z, S_+ and S_- called the Stevens operators [11]. They transform like the symmetry operations of the point symmetry of the site of the rare-earth ion. The b_l^m are empirical coefficients to be determined by experiment.

The parameters of the spin Hamiltonian were evaluated by fitting simultaneously the line positions of all clearly resolved lines, both in the ac and ab planes. An exact diagonalization in combination with a least-squares-fitting procedure in which all resonant EPR line positions, obtained for several orientations of the external magnetic field, were fitted. We have performed three types of fitting: with (i) all b_l^m, $l = 2, 4, 6$; (ii) b_l^m, $l = 2, 4$; (iii) b_l^m, $l = 2$. This was done in order to see how important the higher-order parameters b_l^m ($l = 4, 6$) are for the EPR analysis. The root mean sum of squares of weighted differences between observed and calculated line positions (RMSD) for the fittings (i), (ii) and (iii) are 60, 61 and 107 MHz, respectively. Therefore, the higher-order parameters b_l^m with $l = 4$ significantly improve the RMSD; however, b_l^m with $l = 6$ is negligible. The values of the g-factor and the parameters for all b_l^m ($l = 2$ and 4, $|m| \leqslant l$) are shown in table 1 with the values expressed in GHz. From these values it is clear that the shape of the EPR angular dependence is dominated by the electronic quadrupole tensor. The absolute signs of b_2^0 and b_4^0 were found in the usual way by observing the relative intensities of the EPR lines as a function of temperature [12]. From the measurements at 30 K we found that b_2^0 is negative. The b_l^m values we found are unique for monoclinic site symmetry (see for example the discussion by McGavin, table 4 [13]). The values do not change when using another axis system, only the sign of the b_4^m values are inverted.

The EPR spectra indicate that the Gd^{3+} enters substitutionally into the yttrium site, which has monoclinic point symmetry C_s (see figure 1). Figure 5 shows the projection of a portion of the YF_3 crystal structure in the ac plane. The principal axes X and Z of the electronic quadrupole tensor, which is dominant, are rotated by 30° in relation to the crystallographic axes a and c, respectively. From the EPR angular dependence (figure 3) the principal axis Z of one of the two magnetically inequivalent Gd sites is found at $\theta = 30°$, where the splitting of the EPR lines is largest. The X-axis is chosen perpendicular to Z in the mirror plane ac. Consequently, the Y-axis is coincident with the crystallographic axis b. The principal axis Z of the other magnetically inequivalent Gd ion is found simply by rotation of 120° about the Y-axis (figure 5). The principal axis of the g tensor accompanying the principal axis of the electronic quadrupole tensor. It is interesting to note that its principal value is largest exactly in the direction in which the distance between Gd and the fluorine neighbour is largest.

For monoclinic point symmetry we expect two independent values for the electronic quadrupole tensor, D and E or b_2^0 and b_2^2, respectively, in its principal axis system. However, in our experiment we have rotated the crystal about the crystallographic axes, which are not coincident with the principal axes of the electronic quadrupole tensor. Therefore, off-diagonal

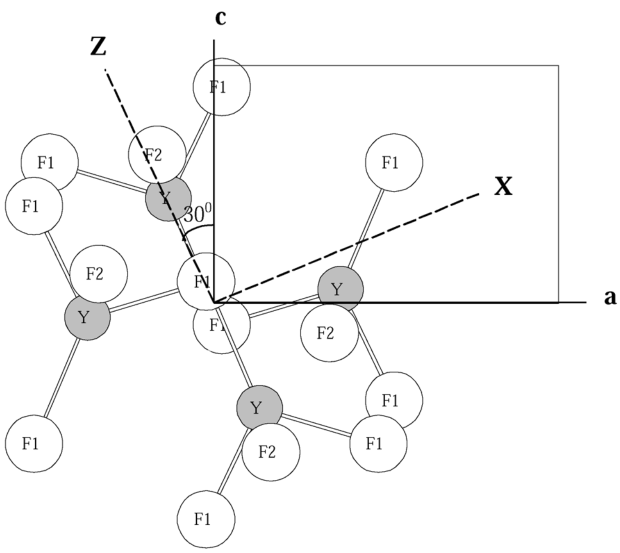

Figure 5. Projection of a portion of the unit cell of YF_3 on the *ac* plane showing four sites of physically equivalent ions. Two of them are magnetically inequivalent. The principal axes *Z* and *X* of the electronic quadrupole tensor are rotated by 30° from the crystallographic axes *a* and *c*, respectively.

elements like b_2^1 and b_2^{-1} are present [13]. The terms b_2^{-2}, b_4^{-2} and b_4^{-4} are also expected and presented in table 1. However, their values are small. For the EPR angular dependence in the *ab* plane (figure 4) we observe seven lines for *B* parallel to the *b* axis. The lines split in doublets when rotating the crystal in the *ab* plane because two of the four physically equivalent ions are magnetically inequivalent in pairs in this plane.

The results of the spin Hamiltonian parameters for Gd^{3+} in YF_3 are compared to EPR studies of Gd^{3+} in similar host crystals of type LaF_3. Misra *et al* [14] have made an EPR study of Gd^{3+} doped single crystals of CeF_3, LaF_3, PrF_3 and NdF_3. They have used the superposition model [15] for the explication of the spin Hamiltonian parameters in these isomorphous hosts with hexagonal structure (LaF_3). In this model the fine structure parameters are related with intrinsic parameters of crystal structure and ionic radii. Taking into account the lack of data for Gd^{3+} in different YF_3-type lattices, it is difficult to find intrinsic parameters from this model. However, the b_2^0 value we have found is about three times larger than that for the hosts studied by Misra *et al* [14]. The coordination number of the gadolinium site is nine for both series; nevertheless the mean distance to nearest-neighbour ligands of the paramagnetic ion is only about five per cent smaller in YF_3. Therefore, the b_2^0 value is unexpectedly high. Further theoretical treatments are under way to understand the interaction of the Gd^{3+} ion with its environment. The appearance of the b_2^1 and b_2^{-1} Stevens parameters can be explained by the fact that the rotation of the crystal was done in the crystallographic crystal system which is not coincident with the principal axis system. However, a small local distortion cannot be ruled out. Electron nuclear double resonance investigations (ENDOR) were tried to give a better understanding of the local structure of the Gd site by the investigation of the fluorine neighbour interactions. The super-hyperfine structure (SHF) of the fluorine is hidden in the line widths of the Gd fine structure lines. The results of the ENDOR investigations will be discussed in a further publication.

5. Conclusion

Our EPR measurements show that the Gd^{3+} rare-earth ion substitutes for Y^{3+} in YF_3. Detailed analysis of the EPR spectra allowed us to determine the fine structure parameters of Gd^{3+} in monoclinic C_s symmetry. The b_2^0 parameter found for Gd^{3+} in YF_3 is unexpectedly high when compared to Gd in the LaF_3 structure and is of the same order as of that for Gd^{3+} in $LiYF_4$, which is known as commercial laser material. For that reason YF_3 doped with rare-earth or transition-metal ions could be also a promising laser host material.

Acknowledgments

We are grateful to Professor Ramayana Gazzinelli for fruitful discussions. One of us, KJG, acknowledges financial support from the Brazilian agency FAPEMIG.

References

[1] Kollia Z, Sarantopoulou E, Cefalas A C and Nicolaides C A 1995 *J. Opt. Soc. Am.* B **12** 782
[2] Hempstead C F and Bowers K 1960 *Phys. Rev.* **118** 131
[3] Scovil H E D, Feher G and Seidel S 1957 *Phys. Rev.* **105** 762
[4] Geschwind S and Remeika J P 1961 *Phys. Rev.* **122** 757
[5] Kollia Y, Srantopoulou E, Cefalas A C, Nicolaides C A, Naumov A K, Semashko V V, Abdulsabirov R Y, Korableva S L and Dubinskii M A 1995 *J. Opt. Soc. Am.* B **12** 782
[6] Rotereau K, Gesland J Y, Daniel P and Bulou A 1993 *Mater. Res. Bull.* **28** 813
[7] Cheethan A K and Norman N 1974 *Acta Chem. Scand.* A **28** 55
[8] Buckmaster H A and Shing Y H 1972 *Phys. Status Solidi* a **12** 325
[9] Feher G and Scovil H E D 1957 *Phys. Rev.* **105** 760
[10] Abragam A and Bleaney B 1970 *Electron Paramagnetic Resonance of Transition Ions* (Oxford: Clarendon)
[11] Zalkin A and Templeton D H 1953 *J. Amer. Chem. Soc.* **75** 2453
[12] Abragam A and Bleaney B 1970 *Electron Paramagnetic Resonance of Transition Ions* (Oxford: Clarendon) ch 3, p 161
[13] McGavin D G 1987 *J. Magn. Reson.* **74** 19
[14] Misra S K, Mikolajczak P and Lewis N R 1981 *Phys. Ver.* B **24** 3729
[15] Misra S K, Mikolajczak P and Korczak S 1981 *J. Chem. Phys.* **74** 922